Monthly Notices of the ROYAL ASTRONOMICAL SOCIETY

MNRAS **450,** 2692–2707 (2015) doi:10.1093/mnras/stv850

G2C2 – III. Structural parameters for Galactic globular clusters in SDSS passbands

Joachim Vanderbeke,[1,2⋆] Roberto De Propris,[3] Sven De Rijcke,[1] Maarten Baes,[1] Michael J. West[2,4] and John P. Blakeslee[5,6]

[1]*Sterrenkundig Observatorium, Universiteit Gent, Krijgslaan 281 S9, B-9000 Gent, Belgium*
[2]*European Southern Observatory, Alonso de Córdova 3107, Vitacura, Santiago, Chile*
[3]*Finnish Centre for Astronomy with ESO (FINCA), University of Turku, Väisäläntie 20, FI-21500 Piikkiö, Finland*
[4]*Maria Mitchell Observatory, 4 Vestal Street, Nantucket, MA 02554, USA*
[5]*Herzberg Insititute of Astrophysics, National Research Council, Victoria, BC V9E 2E7, Canada*
[6]*Department of Physics and Astronomy, Washington State University, 1245 Webster Hall, Pullman, WA 99163-2814, USA*

Accepted 2015 April 15. Received 2015 April 15; in original form 2014 July 30

ABSTRACT

We use our Galactic Globular Cluster Catalog (G2C2) photometry for 111 Galactic globular clusters (GCs) in g and z, as well as r and i photometry for a subset of 60 GCs and u photometry for 22 GCs, to determine the structural parameters assuming King models. In general, the resulting core radii are in good comparison with the current literature values. However, our half-light radii are slightly lower than the literature. The concentrations (and therefore also the tidal radii) are poorly constrained mostly because of the limited radial extent of our imaging. Therefore, we extensively discuss the effects of a limited field of view on the derived parameters using mosaicked Sloan Digital Sky Survey data, which do not suffer from this restriction. We also illustrate how red giant branch (RGB) stars in cluster cores can stochastically induce artificial peaks in the surface brightness profiles. The issues related to these bright stars are scrutinized based on both our photometry and simulated clusters. We also examine colour gradients and find that the strongest central colour gradients are caused by central RGB stars and thus not representative for the cluster light or colour distribution. We recover the known relation between the half-light radius and the Galactocentric distance in the g band, but find a lower slope for redder filters. We did not find a correlation between the scatter on this relation and other cluster properties. We find tentative evidence for a correlation between the half-light radii and the [Fe/H], with metal-poor GCs being larger than metal-rich GCs. However, we conclude that this trend is caused by the position of the clusters in the Galaxy, with metal-rich clusters being more centrally located.

Key words: globular clusters: general.

1 INTRODUCTION

Galactic globular clusters (GCs) are ancient stellar systems (the majority being formed beyond $z \sim 3$), containing of $\sim 10^5$ stars within a volume of ~ 100 pc^3. They provide essential information on the formation and evolution of the Galaxy (e.g. Forbes & Bridges 2010) and are natural laboratories for theories of stellar structure (VandenBerg et al. 2013, and references therein). The structure and properties of GCs bear the imprint of the initial conditions of their formation and interactions with the galactic environment (Brodie & Strader 2006). The high stellar densities (without a dark matter halo) make GCs invaluable objects for the study of N-body dynamics (e.g. Elson, Fall & Freeman 1987; Heggie & Hut 2003; Trenti, Vesperini & Pasquato 2010; Hurley & Shara 2012). We also expect that these complex environments are involved in the formation of several stellar exotica, such as blue stragglers (Ferraro & Lanzoni 2009; Simunovic & Puzia 2014), extreme horizontal branch stars (Fusi Pecci et al. 1992), cataclysmic variables and millisecond pulsars (Benacquista & Downing 2013), intermediate-mass black holes (Lützgendorf et al. 2013) and black hole binaries (Lin et al. 2013).

Structural parameters for GCs are needed to explore correlations between stellar populations, dynamics and the Galactic environment. The Milky Way is the only object where these questions can be explored in detail, as we can resolve clusters to the level of

⋆ E-mail: joachimvanderbeke@gmail.com

individual stars on the main sequence and study their internal kinematics (Frank et al. 2012; Bianchini et al. 2013; Hernandez, Jiménez & Allen 2013; Fabricius et al. 2014; Kacharov et al. 2014). Most structural parameters for Galactic GCs are still measured from surface brightness (hereafter SB) profiles derived from an inhomogeneous compilation of older CCD and photographic data (Trager, King & Djorgovski 1995). The most extensive compilation (McLaughlin & van der Marel 2005) fits these to the classical King (1962, 1966) profile for self-gravitating systems (Wilson 1975 and other profiles are also used). Recently, Miocchi et al. (2013) have derived structural parameters based on star counts from *HubbleSpaceTelescope* (*HST*) and ground-based photometry for 26 clusters. This latter method is arguably the most accurate (e.g. Ferraro et al. 1999, 2003), but it is observationally expensive (e.g. Salinas et al. 2012) and cannot be applied to unresolved systems such as clusters in all but the nearest galaxies (Wang & Ma 2013). As long as the clusters are bright and well populated, we expect that SB profiles will perform adequately (Noyola & Gebhardt 2006 – but, see also Goldsbury, Heyl & Richer 2013). However, in nearly all instances (and almost irrespective of methodology) it is difficult to decide on a 'radius' where GCs 'end'. In several cases, clusters are seen to contain 'extra-tidal' stars (e.g. NGC 1851 – Olszewski et al. 2009; NGC 5694 – Correnti et al. 2011), while tidal tails and other debris are relatively common (e.g. Grillmair et al. 1995; Odenkirchen et al. 2001; Sollima et al. 2011). A further complication is that about 20 per cent of the clusters do not fit smooth King-like models, but exhibit a central density enhancement or core collapse (Cohn 1980). Given the large ages of these objects, this is expected to have occurred in most clusters (Djorgovski & Piotto 1993; Harris 1996), but the formation of hard binaries is expected to halt this process (Vesperini & Chernoff 1994; Fregeau & Rasio 2007).

We have recently completed multiwavelength observations in the Sloan Digital Sky Survey (SDSS) *ugriz* passbands for the bulk of the southern Galactic GCs and supplemented these data with northern clusters from the SDSS DR9 (York et al. 2000; Ahn et al. 2012). This results in a total data set with *g* and *z* photometry for 111 GCs, as well as further *r* and *i* photometry for 60 clusters and *u*-band imaging for 22 GCs. We have presented a study of the integrated *griz* aperture magnitudes and colours for these objects in Vanderbeke et al. (2014a, hereafter Paper I) and used these colours to improve colour–metallicity relations in Vanderbeke et al. (2014b, hereafter Paper II), the first two papers in this series. Here, we use the imaging to produce SB profiles and derive structural parameters by fitting King models to our homogeneous survey of the Galactic GC system. The G2C2 survey has some clear advantages when compared to previous studies: our data are uniform, the measurements are based on CCD imaging and the clusters are observed during photometric nights (Paper I). Moreover, our data cover the bulk of the Galactic GCs, were taken in the popular SDSS filter system and were analysed carefully and homogeneously.

The paper is organized as follows. In Section 2, we describe the data. Section 3 reports on our analysis, presents the structural parameters and compares those with previous work. At this stage, we simulate mock clusters to test our fitting algorithm and explore possible sources for parameter biases. We discuss the observational biases in more detail and use the large images for the clusters from the SDSS (which theoretically can be studied to any radius) to study the limitations of our data set by artificially constraining the extent of the SDSS SB profiles. We also scrutinize the effects of bright red giant stars on the centring of cluster profiles and its consequences for the SB profiles and the King model fits, which further confirm the findings based on the mock data. In Section 4, we compare our King (1962) parameters with studies from the literature using both SB and count density profiles. In Section 5, we discuss our results and explore their significance for internal colour gradients, stellar populations and the interactions of clusters with our Galaxy. Finally, in Section 6 we summarize our conclusions.

2 DATASET

The data set for this paper is based on the Galactic Globular Cluster Catalog (G2C2): a homogeneous imaging survey of a large fraction of the Galactic GC system in the SDSS passbands. Paper I details the data acquisition process and describes how these data were reduced. That study also presented our procedures to correct for contamination, how we deal with extinction and calibrate photometry. We refer to the above paper for details, but give here a short summary of the essential information. The bulk of the observations were carried out on the Cerro Tololo Inter-American Observatory (CTIO) 0.9 m telescope in a series of observing runs between 2003 and 2013, with most of the data coming from the 2004 June season. We performed the standard CCD reduction procedures and cosmic ray removal, followed by calibration on the SDSS system using stars from Smith et al. (2002). For all clusters, we have *g* and *z* photometry, often taken on several different nights, while for an important subset we also have *r* and *i* imaging. We supplemented this with available clusters within the SDSS footprint (Ahn et al. 2012). This resulted in a total sample of 111 GCs with *gz* photometry and 60 GCs with *ri* photometry.

In Paper I, we used these data to calculate aperture photometry within the (literature) half-light radius (from the 2010 edition of the Harris 1996 compilation, which is the version we will use throughout this study). This required us to deal with estimating the sky level from CTIO images that do not reach to the cluster tidal radius. As this is an important issue for the present paper, we discuss this further below. We also adaptively searched for the cluster centre and we similarly describe this in greater detail in this paper. Moreover, we experiment in the current study with a new centring method based on red giant branch (RGB) stars in Section 3.3. Finally, we carried out removal of contaminating (foreground) stars to obtain clean aperture magnitudes and corrected for extinction using the most recent values from Schlafly & Finkbeiner (2011). However, in Paper II we found some evidence that these extinction values may suffer from systematic errors, especially near the plane and the Galactic bulge.

For several GCs in Paper I, we were unable to carry out aperture photometry because bright red giants in the unresolved cluster centres saturated the CCD. Our purpose in the above publication was to provide a conservative set of aperture magnitudes and colours, and we therefore excluded a number of clusters from our analysis. Here, we fit King models to the SB profiles and we are able to apply an iterative clipping method and profile fitting to derive 'model' magnitudes.

3 STRUCTURAL PARAMETERS

3.1 SB profiles

We derive radial SB profiles for all clusters and all passbands by using conventional aperture photometry, in annuli of increasing radius, similar to the procedure of building a curve of growth for extended systems. For the CTIO 0.9 m data, where the field of view is 13.6 arcmin on the side, the annuli are 15 pixels (corresponding

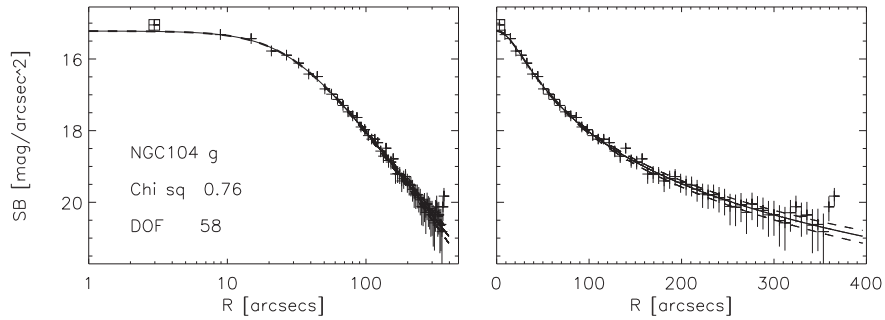

Figure 1. SB distribution of NGC 104 in the *g* band. The left-hand panel focuses on the inner region of the cluster, while the right-hand panel gives details on the outer regions. The dashed lines show the 1σ deviation of the model, with squares representing the data points that have been clipped iteratively.

to ∼5.9 arcsec) wide, or approximately four times the seeing disc. We integrated to the edges of the images to obtain the SB profiles to the ∼6.5 arcmin limit allowed by the CTIO 0.9 m field of view (FOV). For SDSS data, we can theoretically integrate the profile to infinity, but we also simulate observations limited to the 4.2 and 6.5 arcmin field of view used for all other clusters to test the effects of the limited aperture on structural parameters.

We fit the SB profile to a King (1962) model of the form:

$$\mathrm{SB}(r) = k\left(\frac{1}{[1+(r/r_\mathrm{c})^2]^{1/2}} - \frac{1}{[1+(r_\mathrm{t}/r_\mathrm{c})^2]^{1/2}}\right)^2, \quad (1)$$

where r is the aperture radius, r_c is the core radius and r_t the tidal radius. The constant k is related to the central SB μ as

$$\mu = k\left(1 - \frac{1}{[1+(r_\mathrm{t}/r_\mathrm{c})^2]^{1/2}}\right)^2.$$

We fit these using a Levenberg–Marquardt non-linear least squares algorithm (Press & Schechter 1974; Bevington & Robinson 1992). We define a concentration index $c' = r_\mathrm{t}/r_\mathrm{c}$ to simplify our numerical work, while $c \equiv \log(r_\mathrm{t}/r_\mathrm{c})$ as in McLaughlin & van der Marel (2005). We iterated the fit with 5σ clipping about each SB point to remove the effects of bright contaminating stars. We also truncate the SB profiles, excluding the SB points which are outside the tidal radius of the previous iteration. Therefore, the outer regions of the SB profile were clipped out for some very faint clusters, hence the final fit did not rely on the full 6.5 arcmin SB profile. The iteration process was stopped when the input SB profile vector did not change anymore when compared to the one of the previous loop. As a consequence of the 5σ clipping, the central SB point was also ignored in some cases, mostly when the SB profile was centred on bright RGB stars.

We show an example King profile for the classical rich cluster NGC 104 (47 Tucanae) in Fig. 1. Fits for all other objects are placed in an online appendix. This rich massive cluster extends much further than our limited FOV, thus the concentration index cannot be reliably estimated. It is very difficult in any case to constrain the tidal radii (and the related concentrations) accurately. Since the field of view of CTIO data does not reach to the tidal radius for most if not all clusters in the sample, it is inherently difficult to measure this quantity. We therefore used an ad hoc estimate, adopting as the tidal radius the radius at which the best fit King profiles had flux comparable to the mean sky noise. For clusters within SDSS, determining the tidal radius is, in principle, not a problem, since one can extrapolate the flux to large distances; even in this case, the tidal radius is often difficult to determine (Jordán et al. 2009).

We tabulate the derived parameter values based on the CTIO data in Table 1. The entire table can be found in the online appendix. We estimated the errors on these parameters by bootstrapping the derived fits with 100 random points (assuming Poisson errors) and deriving new King model fits to these artificial data. The errors in the table are the 1σ conditional errors on each parameter. Where we have more than one observation in one or more filters, we always list the King parameters based on the longest one in Table 1 or (for similar observing times) the best reduced χ^2. Note that in some cases (e.g. core-collapsed systems), we were forced to exclude the inner annulus from our analysis as it would otherwise drive the whole fit because of its small errors: we exclude the central SB point when it was more than 1 mag brighter than the four adjacent SB points. One example is NGC 5927 in the upper panel of Fig. 2. This could bias the results for core-collapsed clusters. However, these clusters are by definition not well represented by King models in any case.

We now integrate the King profiles numerically to compute a 'model' magnitude within the half-light radius. These are also given in Table 1. For SDSS clusters we give model and aperture magnitudes in Table 2: the full table is available online, while an extract is shown here for guidance. In Paper I, we presented aperture magnitudes based on the half-light from Harris (1996). Here, we determine the half-light radius and we therefore choose to compare the model and aperture magnitudes. Generally, these magnitudes agree well, with a median magnitude difference (model−aperture) of ∼0.01 mag.

3.2 Sky values

In order to follow globular cluster profiles to low SB levels, an accurate estimate of the sky value is necessary. Small errors in sky values propagate because of the large areas of the apertures, especially in the outer regions of each cluster. We have used the MMM (Mean, Median, Mode) algorithm to measure the sky flux in apparently blank regions in the corners of the CCD images: the routine is adapted from DAOPHOT (Stetson 1987), specifically developed for crowded fields as in our GCs. The algorithm clips sky pixels well above the median and combines median, mean and mode sky values to obtain a more accurate background estimate. In our case, exposure times are relatively short to preserve the dynamic range between the bright central regions and the low SB wings of the cluster profile; this leads to more uncertain sky determinations (see Paper I for more details). One can compare this with the most commonly used approach to derive SB profiles for galaxies (Peng et al. 2002, 2010): in some cases the outskirts of extended systems are barely above the sky noise and even the areal increase in the apertures is offset

Table 1. Extract of the King parameter table based on CTIO SB profiles. Central SB uncertainties are pure bootstrapping uncertainties and do not include calibration uncertainties, neither the systematic error introduced in. We do not list the King model concentration c, because this parameter could not be estimated reliably based on our data. Table 3 presents the systematic errors on each of the parameters. Model and aperture (Aper) magnitudes are computed within the listed r_h. In case of multiple observations, the longest observation was chosen (with exposure time ExpT). The reduced χ^2 and the degrees of freedom (DOF) of the fit are also given. $SB0_{in}$ indicates if the central SB point was included by the final fit.

ID		μ_0 (mag arcsec^{-2})	$\sigma(\mu_0)$	r_c (′)	$\sigma(r_c)$	r_h (arcmin)	$\sigma(r_h)$	Model ([mag)	Aper (mag)	ExpT (s)	χ^2	DOF	$SB0_{in}$
NGC104	*g*	14.94	0.00	0.47	0.00	2.62	0.01	5.09	5.08	60	0.76	58	0
NGC104	*z*	13.82	0.00	0.51	0.00	2.52	0.01	3.89	3.85	60	1.32	56	1
NGC288	*g*	20.31	0.00	1.76	0.03	2.19	0.02	9.14	9.12	270	0.99	58	0
NGC288	*r*	19.91	0.01	2.03	0.07	2.05	0.03	8.76	8.70	60	0.57	58	0
NGC288	*i*	19.68	0.01	2.32	0.12	2.01	0.01	8.49	8.41	60	0.55	58	0
NGC288	*z*	19.56	0.01	2.51	0.17	1.88	0.02	8.44	8.39	60	0.21	58	0
NGC362	*g*	15.07	0.00	0.18	0.00	0.97	0.01	7.39	7.35	60	0.44	60	1
NGC362	*r*	14.39	0.00	0.17	0.00	0.80	0.01	6.89	6.92	60	0.48	59	1
NGC362	*i*	14.08	0.00	0.17	0.00	0.83	0.01	6.54	6.58	60	0.56	59	1
NGC362	*z*	13.90	0.00	0.18	0.00	0.70	0.01	6.45	6.50	60	0.28	59	1

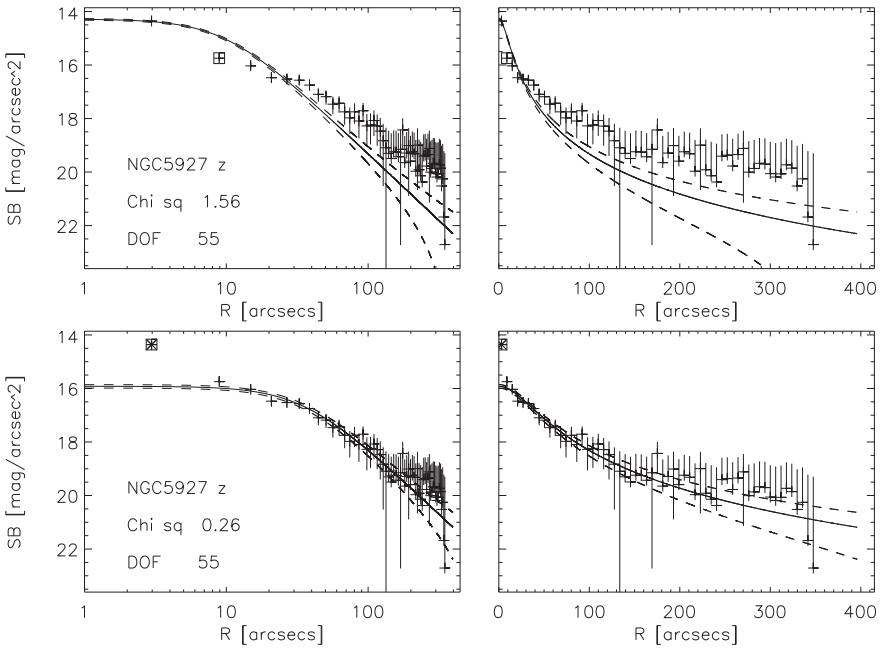

Figure 2. SB distribution for NGC 5927 in the z band. Legend as in Fig. 1. The upper panel shows the fit with natural ($1/\sigma$) weighting, the lower panel excludes the central SB point because it is more than 1 mag brighter than the four adjacent SB points. The asterisk for the central SB point indicates that it was not considered in any of the fitting steps. Boxes indicate the SB points that were not considered in the final fit.

by the increasing noise from the sky, flat-field and detector read. This may lead to a bias in favour of low effective radii. The problem may be further complicated by our assumption of circular symmetry, whereas there is evidence of changing ellipticity and position angles in the outer regions of some GCs (Bianchini et al. 2013). Additionally, some clusters have stars beyond the tidal radius, while others underfill their tidal region (Gieles et al. 2010; Alexander & Gieles 2013). Peng et al. (2002, 2010) argues for the solution we have eventually chosen, to estimate the sky independently and hold it fixed for the estimate. Finally, in some cases, some very bright (sometimes saturated) foreground stars were replaced by the sky value. Generally, these stars were already clipped by our fitting algorithm. However, the model fits and residuals look nicer when masking these saturating foreground stars. It is particularly useful to do this for faint sparse clusters, which are sometimes not much brighter than the sky itself.

3.3 Centering errors

An essential element in our procedure is the choice of an appropriate centroid for the apertures. In Paper I, we determined the cluster centre by using a series of small apertures surrounding the optical centre and choosing the position where the flux is maximal (Noyola & Gebhardt 2006; Bellazzini 2007). As a first approximation, this is our estimate of the position of the cluster centre. During the analysis of the data, it became clear that a few bright stars (mostly RGB stars) can strongly affect the derived parameters, mostly because of their effect on the position of the cluster centre (Goldsbury et al. 2013) and

Table 2. Extract of the GC King parameters and errors for SB profiles based on SDSS data.

ID		μ_0 (mag arcsec^{-2})	$\sigma(\mu_0)$	r_c (arcmin)	$\sigma(r_c)$	r_h [arcmin)	$\sigma(r_h)$	Model (mag)	Aper (mag)	χ^2	DOF	$SB0_{in}$
NGC2419	*u*	20.95	0.01	0.34	0.05	0.60	0.04	12.78	12.76	0.05	49	1
NGC2419	*g*	19.79	0.00	0.36	0.00	1.15	0.00	10.91	10.99	0.76	52	1
NGC2419	*r*	19.33	0.00	0.36	0.00	1.22	0.00	10.41	10.48	0.61	52	1
NGC2419	*i*	19.10	0.00	0.37	0.00	1.19	0.00	10.17	10.23	0.78	52	1
NGC2419	*z*	19.01	0.01	0.37	0.01	0.80	0.01	10.45	10.47	0.08	50	1
NGC5024	*u*	18.89	0.00	0.45	0.00	0.85	0.01	10.11	10.11	0.06	42	1
NGC5024	*g*	17.59	0.00	0.41	0.00	1.07	0.01	8.68	8.68	0.73	52	1
NGC5024	*r*	17.10	0.00	0.38	0.00	1.10	0.01	8.26	8.26	1.23	53	1
NGC5024	*i*	17.19	0.00	0.45	0.00	1.08	0.01	8.16	8.15	0.67	53	1
NGC5024	*z*	16.67	0.00	0.39	0.00	0.92	0.01	7.97	7.96	0.59	50	1
NGC5053	*u*	23.52	0.04	2.32	0.96	1.06	0.01	13.41	13.37	0.01	56	1
NGC5053	*g*	22.43	0.01	2.65	0.31	2.34	0.03	10.91	10.88	0.25	56	1
NGC5053	*r*	22.09	0.01	2.59	0.31	2.24	0.02	10.65	10.65	0.30	51	1
NGC5053	*i*	21.88	0.01	2.79	0.29	2.41	0.05	10.27	10.24	0.36	56	1
NGC5053	*z*	21.81	0.02	2.93	0.87	1.65	0.01	10.80	10.74	0.10	56	1

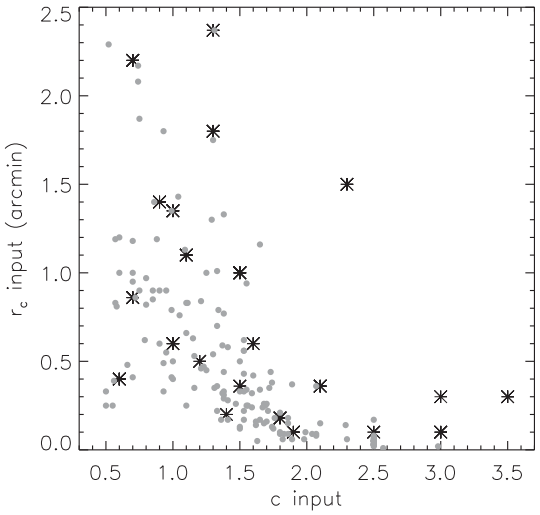

Figure 3. Distribution of the input r_c and c parameters for the IRAF mock data. Black asterisks represent our input parameters, small filled grey circles show the literature values (Harris 1996).

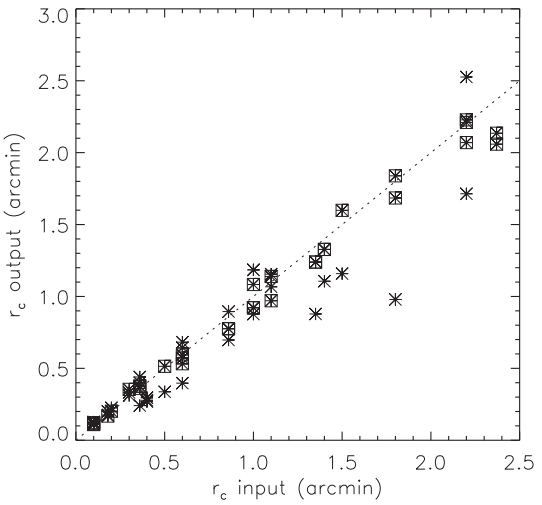

Figure 4. Comparison of the input core radii r_c with the resulting r_c based on our fitting algorithm. Well-populated clusters ($N = 10^5$) are indicated with a box, other clusters are more sparse ($N \leq 10^4$). The dotted line shows the one-to-one correspondence.

especially for poorer systems. Fitting the centres of GCs accurately has basically been an issue ever since King models were fitted to SB profiles. Djorgovski & King (1986) found that about one-fifth of GC cores are not well fit even with high-concentration King models. Collapsed cores, which are better represented by power-law profiles, are encountered frequently. We tested this by creating some mock clusters using IRAF.[1]

Stars were generated using the Bahcall & Soneira (1980) stellar luminosity function and distributed over the CTIO FOV according to the spatial probability distributions determined by different King model density distributions. Fig. 3 shows the distribution of the input r_c and c in the IRAF procedure. These input parameters cover the known values from the literature (Harris 1996) well and are extended to somewhat higher concentrations. Because the sampling of the clusters can affect the SB profile determination, two approaches were used for the stellar densities: images of well-populated clusters and two-dimensional projections of clusters with 10^5 stars, while more sparse clusters only contain 10^4 stars. Obviously, the resulting observed density of the cluster does depend on r_c and c itself. No foreground or background contamination is included. Exposure times, which determine the signal-to-noise of the mock data, were chosen to match our real observations. To derive the cluster centre, we used the above described procedure from Noyola & Gebhardt (2006) and Bellazzini (2007).

For well-populated clusters measured core radii agree well with the input values (Fig. 4). For sparser clusters, the agreement is worse, with some showing large offsets. A strong outlier (input $r_c \sim 1.8$ arcmin, output $r_c \sim 1$ arcmin) shows how stochastic effects may affect our results. We generated this mock GC with 10^4 stars, hence it is sparsely populated. In fact, the SB profile was centred on a bright star, resulting in a strong artificial central peak. This led to a large overestimate of the concentration index. If we exclude, arbitrarily, the central SB point, this yields more reasonable values.

In Fig. 5, we compare the IRAF input concentrations with the output of the fitting algorithm. We find that a significant fraction

[1] IRAF is distributed by the National Optical Astronomy Observatory, which is operated by the Association of Universities for Research in Astronomy under cooperative agreement with the National Science Foundation.

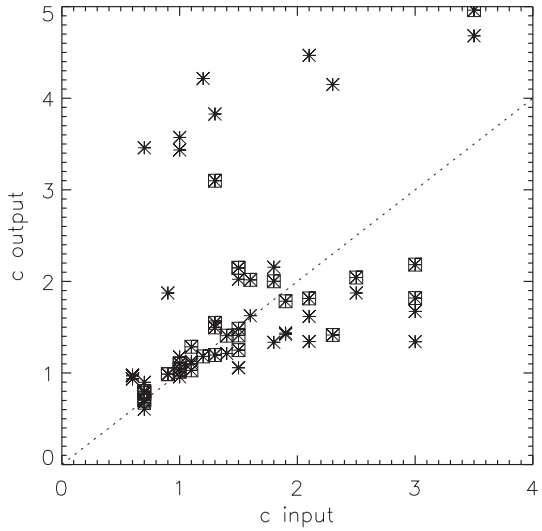

Figure 5. Comparison of the IRAF input concentrations with the resulting output c based on our fitting algorithm. Legend as in Fig. 4. Due to the limited FOV, the concentrations can be overestimated: $c \gtrsim 2.5$ are not reliable. See text for more details.

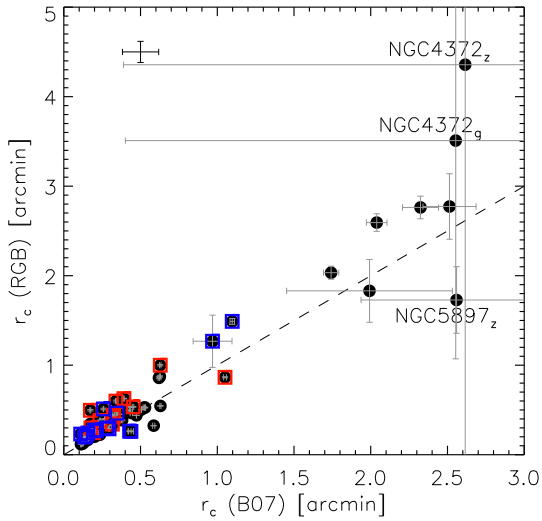

Figure 6. Comparison of the core radii r_c based on SB profiles obtained with the roaming procedure (Bellazzini 2007, hereafter B07) and RGB-based centres. The red squares indicate the 'red core' clusters (with $\Delta_{g-z} > 0.1$, defined in Section 5.5). Blue squares indicate the 'blue core' clusters (with $\Delta_{g-z} < -0.2$). The black error bars in the top-left corner show the z-band systematic error. See text for more details.

of the simulated clusters show large concentration discrepancies, especially for sparsely populated clusters. For GCs with tidal radii much beyond the FOV, it is impossible to constrain the concentrations, which is not surprising. In general, the output concentrations larger than about 2.5 are not reliable.

Because the distribution of bright stars is stochastic and the central SB distributions of King models are flat, errors in the centring may lead to artificially flat profiles (Mackey & Gilmore 2003). Sometimes, however, uncertainties in determining the cluster centre can also produce artificially *peaked* profiles. Therefore, we also experimented with an alternative centring method, using the weighted mean position of cluster red giants to determine the centre of the cluster. We expect that the red giants stars are equally distributed

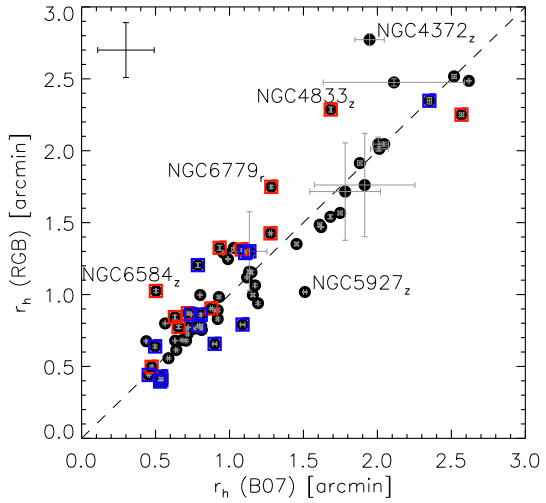

Figure 7. Comparison of the half-light radii r_h based on SB profiles obtained with the roaming procedure (Bellazzini 2007, B07) and RGB-based centres. Legend as in Fig. 6. See text for more details.

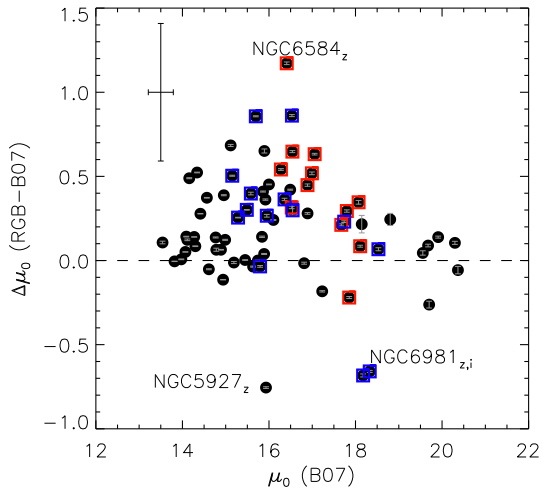

Figure 8. Comparison of the central SB based on SB profiles obtained with the roaming procedure (Bellazzini 2007, B07) and RGB-based centres. Legend as in Fig. 6. See text for more details.

around the centre, hence this method should not be biased by the stochastic positions of some bright stars. Because this method removes 'artificial' peaks or dips in the SB profile (Miocchi et al. 2013), it is found that the core radii increase with respect to our original method.

In Figs 6–8, we compare the core, half-light and central SB derived using our original approach and a centre based on the positions of red giant stars. The half-light radii compare well between the two approaches, while the central SB decreases as artificial peaks in the profile are removed.

From this, we estimate the systematic error on the parameters introduced by the uncertainty in determining the cluster centre and list the corresponding values in Table 3.

3.4 Effects of a limited field of view

We compare clusters in common between the SDSS and our CTIO data. In principle, there is no limit to how far a cluster can be followed with SDSS photometry and therefore we can test how our

Table 3. Systematic errors for the structural parameters due to the stochastically distributed RGB stars and the uncertainty on the centre determination. For the *ri* parameters, the systematic uncertainties for the *z* band should be adopted for all parameters. See text for more details.

Filter	$\sigma_{\rm syst}(\mu_0)$ (mag arcsec^{-2})	$\sigma_{\rm syst}(r_{\rm c})$ (arcmin)	$\sigma_{\rm syst}(r_{\rm h})$ (arcmin)
g	0.228	0.077	0.101
z	0.289	0.118	0.191

limited FOV affects model parameters. Note, however, that even SDSS data have their limitations: bright RGB stars can saturate the SDSS CCD; moreover, the mosaicking of the SDSS data can result in artificial sky gradients.

We use the SDSS mosaics to determine the SB profile and fit this to a King model. We then artificially restrict the field to radii of 4.2 and 6.5arcmin (the total CTIO FOV), to estimate the influence of the field of view on the model fits. In general, we find that the smaller field of view biases the results towards a smaller core radius, but using the full 6.5 arcmin FOV solves this issue (Fig. 9). Note that tidal tails were found in NGC 5053 (Jordi & Grebel 2010).

In Fig. 10, we present a comparison of the half-light radii based on the full mosaicked SDSS frame and the artificially truncated profiles. These two quantities compare well, which suggests that the half-light radius is also generally well determined. The scatter on the one-to-one correspondence is again reduced when using the 6.5 arcmin SB profile instead of the 4.2 arcmin SB profile.

Fig. 11 shows a comparison of the structural parameters for clusters with both SDSS (full images) and CTIO data. The central surface brightnesses are in good agreement (with one exception – NGC 7078 – whose profile is notoriously difficult to fit – Newell & Oneil 1978). Core radii are also in good agreement, while concentrations from our data are generally found to be unreliable.

3.5 Comparison of observations in the *gz* filters

Different filters are sensitive to different stars. However, if the King parameters truly reflect the star count densities, we do not expect substantial differences between the structural parameters based on observations in the blue or red.

Fig. 12 compares the core radii and half-light radii based on the *g* and *z* filters. We do not find evidence for a systematic trend in the core radius or the half-light radius.

GCs close to the Galactic plane are known to suffer from differential reddening (Alonso-García et al. 2011). Observations taken at longer wavelengths are less affected by the extinction. Therefore, we expect a correlation between the differential reddening and the *gz* structural parameter differences, if the differential reddening plays a significant role in the determination of the King parameters. However, we do not find any correlation and conclude that the differential reddening does not strongly bias our parameter determinations.

4 COMPARISON WITH THE LITERATURE

We now compare our results with previous determinations of structural parameters from the literature. First, we compare with the 2010 edition of Harris (1996), which is largely a compilation of the McLaughlin & van der Marel (2005) SB profile study. Then, we also compare with the results of Miocchi et al. (2013) who used star count density profiles to determine the structural parameters.

It is clear that some clusters have lower quality data, resulting in more uncertain parameters. We therefore restrict our analysis to a smaller, 'clean' sample where we can trust our determinations of the main structural parameters. We impose following constraints:

(i) $r_{\rm c} > \sigma(r_{\rm c})$: the core radius has to be significantly different from zero (based on the bootstrap errors, not including the systematic errors).

(ii) $\mu_0 < 20$ mag/ arcsec^2: clusters fainter than this SB have very large photometric errors. SB points are often not significantly different from zero.

These conditions are met for 12, (80, 41, 42 and 87) in the *u* (*g*, *r*, *i*and*z*, respectively) band. We have experimented with SB criteria including the effects of foreground extinction (basically imposing magnitude limits on the apparent SBs, not corrected for extinction), but this did not strongly affect the selected clusters for

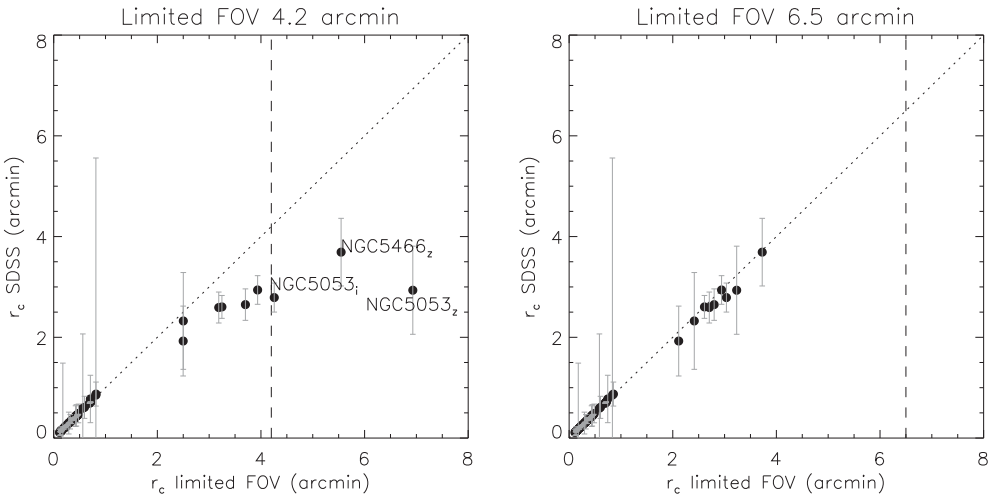

Figure 9. Comparison of the core radii $r_{\rm c}$ based on the full mosaicked FOV and artificially limited SB profiles of 4.2 and 6.5 arcmin (left- and right-hand panel, respectively) for all SDSS GCs belonging to the clean sample introduced in Section 4 (e.g. 19 GCs for *g* and 18 GCs for *z*). The artificial cuts limiting the SB profile radius are indicated with the dashed lines. The dotted line represents the one-to-one correspondence. It is clear that the scatter is significantly reduced using the 6.5 arcmin SB profiles, stressing the importance of using the entire CTIO FOV. See text for more details.

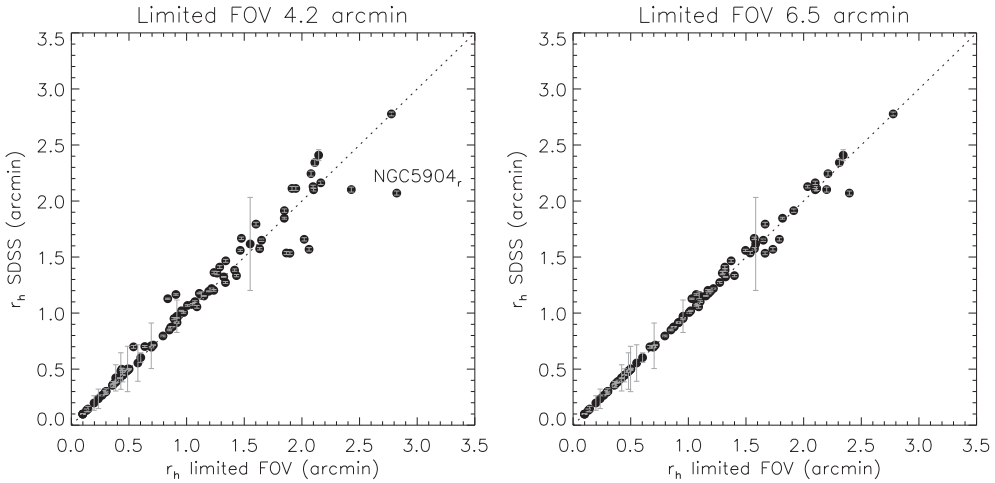

Figure 10. Comparison of the half-light radii r_h based on the full mosaicked FOV and an artificial limited SB profile for the SDSS GCs belonging to the clean sample introduced in Section 4 (e.g. 19 GCs for g and 18 GCs for z). The dotted line represents the one-to-one correspondence. It is clear that the scatter is reduced using the 6.5 arcmin SB profiles, stressing the importance of using the entire CTIO FOV. See text for more details.

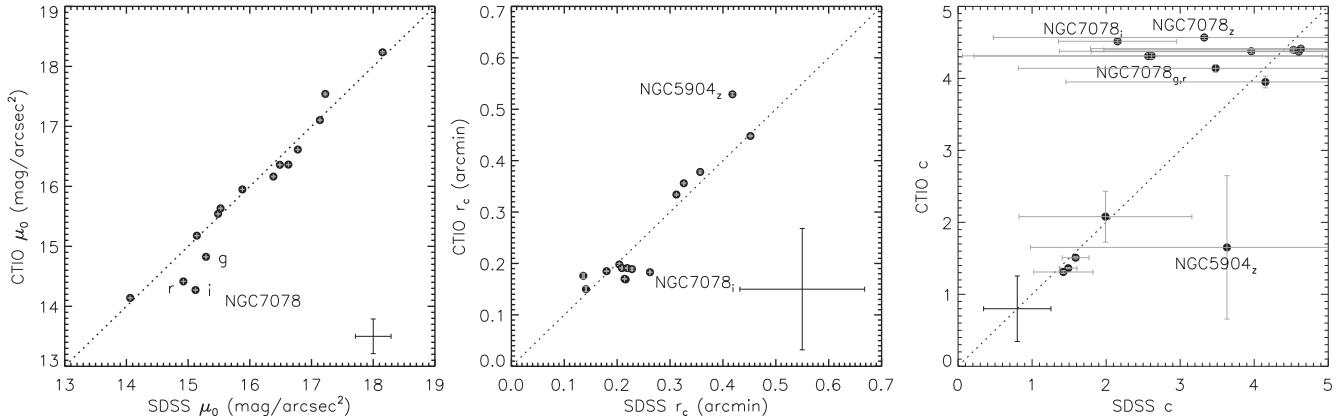

Figure 11. Comparison of the King model parameters (central SBs μ_0, core radii r_c and concentrations c) based on the full mosaicked SDSS FOV and on the CTIO data. The dotted line represents a one-to-one correspondence. The z-band systematic errors are shown by black error bars.

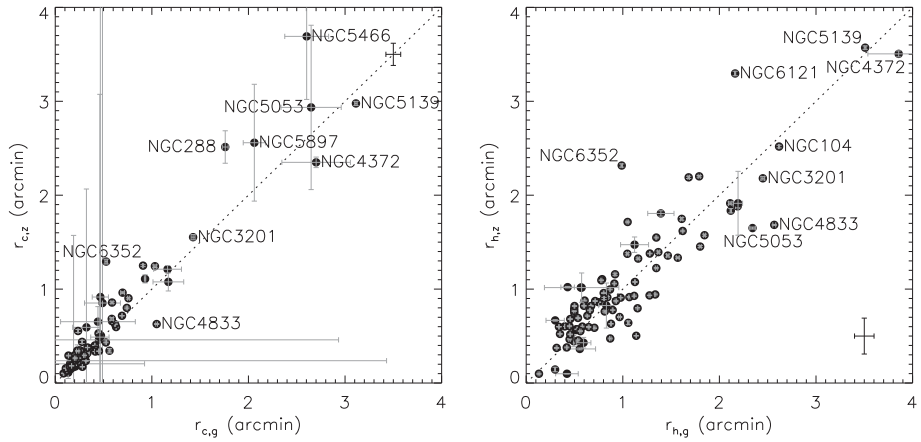

Figure 12. Comparison of the King parameters derived based on observations with the g and z filters. The black error bars present the corresponding systematic errors, as listed in Table 3.

the clean sample. Therefore, we do not introduce restrictions on the foreground extinction as this would automatically exclude all GCs close to the Galactic plane. However, some disc/bulge clusters were removed from the sample, either because of the strong stellar contamination or because of the low apparent SB points (often not significantly higher than the sky, partly due to the foreground extinction). Because the number of clusters is largest in the gz bands, we will focus on these filters during the analysis and discussion.

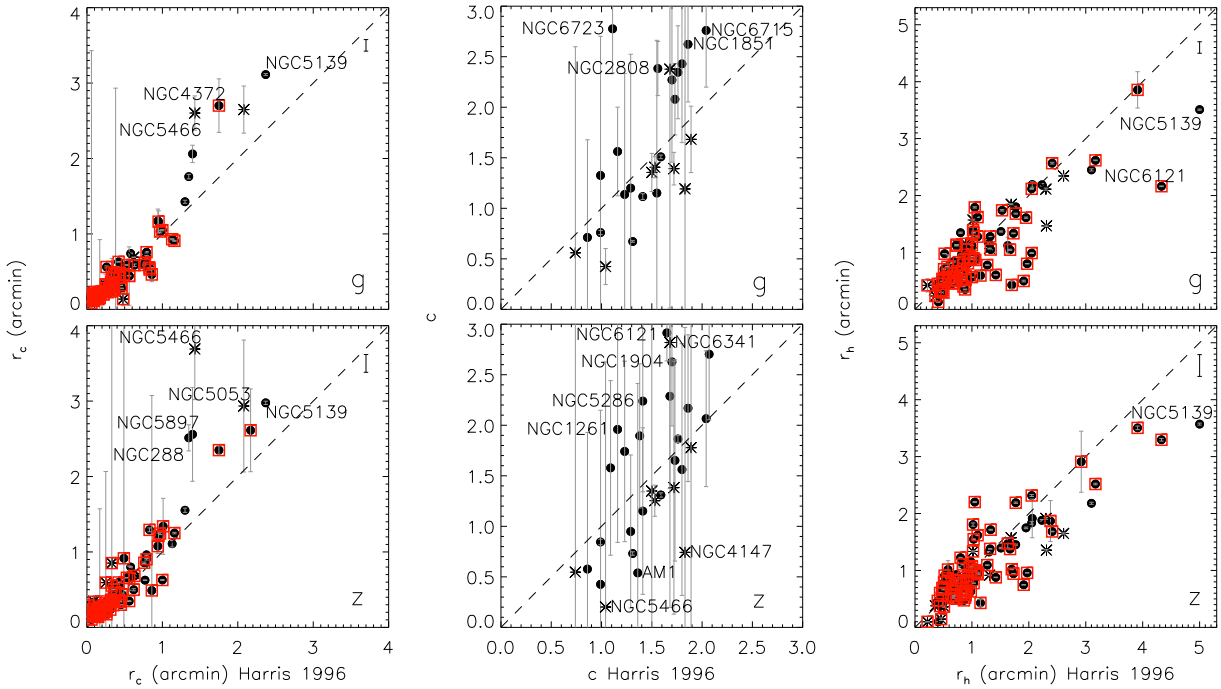

Figure 13. Comparison of the structural parameters between our results (for the g and z band) and the literature (Harris 1996). Filled circles are values based on CTIO SB profiles, supplemented with SDSS values represented by asterisks. The dashed line indicates the one-to-one correspondence. High-concentration clusters (with $c \geq 2.5$) are indicated with red boxes in the left- and right-hand panels. Concentrations higher than ∼2.5 are unreliable, which was also concluded from the simulations in Fig. 5. Therefore, clusters with $c > 3$ are not included in the concentration panel. However, both r_c and r_h are recovered well for the bulk of the cluster sample. The systematic error (given in Table 3) is illustrated by the black error bar in the top-right corner of each panel. See text for more details.

4.1 Comparison to parameters based on SB profiles

Fig. 13 compares r_c, c and r_h to the literature (Harris 1996). The left-hand panel of the figure compares the core radii (based on the g and z bands). The match for the well-populated clusters is very good, with the exception of NGC 5139. For this cluster, our fitting algorithm clipped the central SB point (for both g and z filters), which accounts for the larger value of the core radius. However, for poor clusters (indicated in the figure), our resulting r_c can be biased. The middle panel compares our concentrations with Harris (1996). For the bulk of our sample, the concentrations are unreliable and will therefore not be discussed further.

In the right-hand panel of Fig. 13, we show our half-light radii versus the values in the Harris (1996) compilation. For smaller clusters ($r_h \lesssim 1$ arcmin), the data fall close to the 45° line, albeit with somewhat large scatter. For clusters subtending a larger angle on the sky, we find that our r_h are systematically lower, probably because of our poorer value of r_t or a poor sky determination (see Section 3.1).

As an additional check, we selected a representative subsample of CTIO clusters and fitted Sérsic profiles in pixel space with BUDDA (de Souza, Gadotti & dos Anjos 2004; Gadotti 2008). Again, we found that the effective Sérsic radius (equivalent to the radius encompassing half of the cluster light) was significantly smaller (about a factor of 3) than the literature values. Both approaches suffer from the sky determination issues related to the limited FOV of the CTIO data. Nevertheless, the centre determination is incorporated in the BUDDA fitting algorithm, hence we do not expect a strong bias due to central RGB stars.

The King model parameters are fitted simultaneously. Therefore, the discrepancies between the resulting parameters and the values given by Harris (1996) could be correlated. In Fig. 14, we study these correlations in more detail and conclude that no correlations between Δr_c, Δr_h and Δc are present.

4.2 Comparison to star count density profiles

Star count density profiles mainly trace the abundant main-sequence stars in GCs. SB profiles are vastly affected by bright evolved RGB stars, that sink to the cluster centre due to mass segregation (Fregeau et al. 2002). In contrast to SB profiles, star count profiles are not biased by the presence of sparse, bright stars (Noyola & Gebhardt 2006). Therefore, the latter are believed to be the most reliable way to determine structural parameters. However, our CTIO and SDSS data does not have the required resolution to derive such radial stellar density profiles. Based on a combination of high-resolution *HST* observations and ground-based observations, Miocchi et al. (2013) were able to construct star count profiles and derived structural parameters for 26 Galactic GCs.

Fig. 15 presents a comparison between our King model parameters and the parameters derived by Miocchi et al. (2013). Our concentrations, shown in the left-hand panels, again prove unreliable. The middle panels compare our newly derived core radii with the core radii derived by Miocchi et al. (2013) based on King model fits to star count density profiles. In general, these compare well, with some exceptions which are indicated in the figure. The right-hand panels of Fig. 15 show a comparison between our King model r_h and the effective radii r_e derived by Miocchi et al. (2013). The scatter is rather large with some significant outliers.

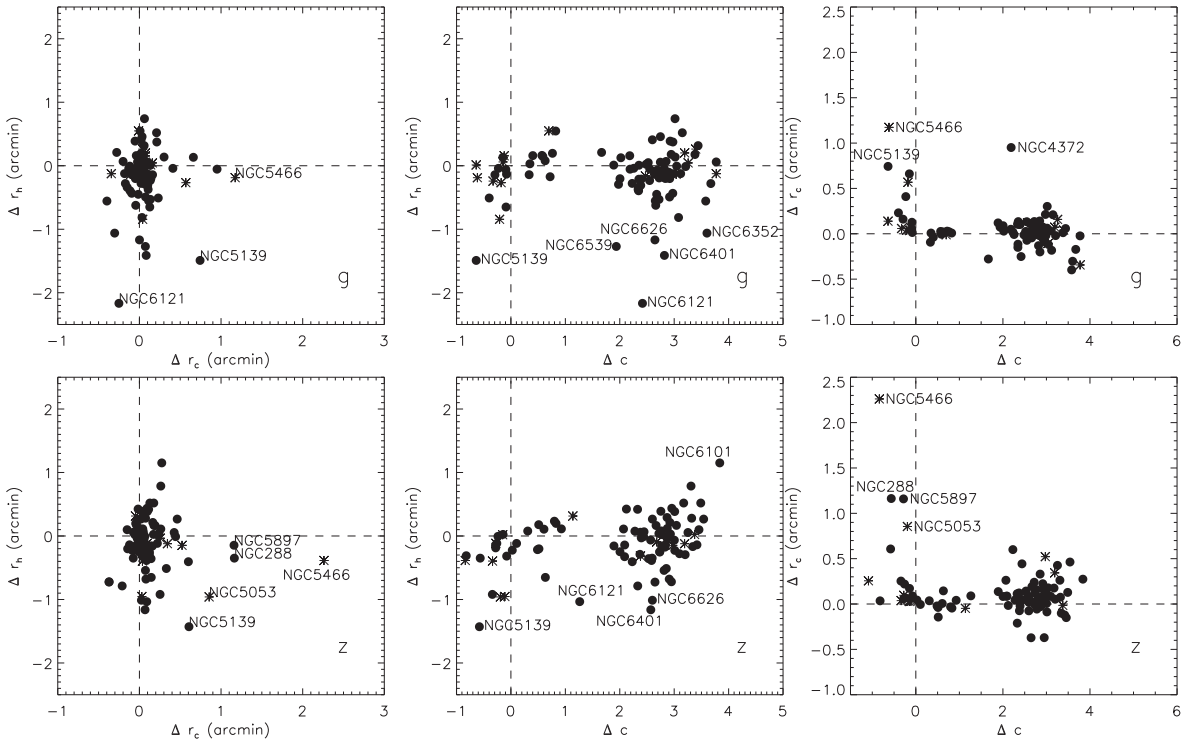

Figure 14. Correlations between the differences of the King parameter determinations when compared to the literature ($\Delta p = p_{\rm thiswork} - p_{\rm Harris\ 1996}$ for $p = r_{\rm c}$, c, $r_{\rm h}$).

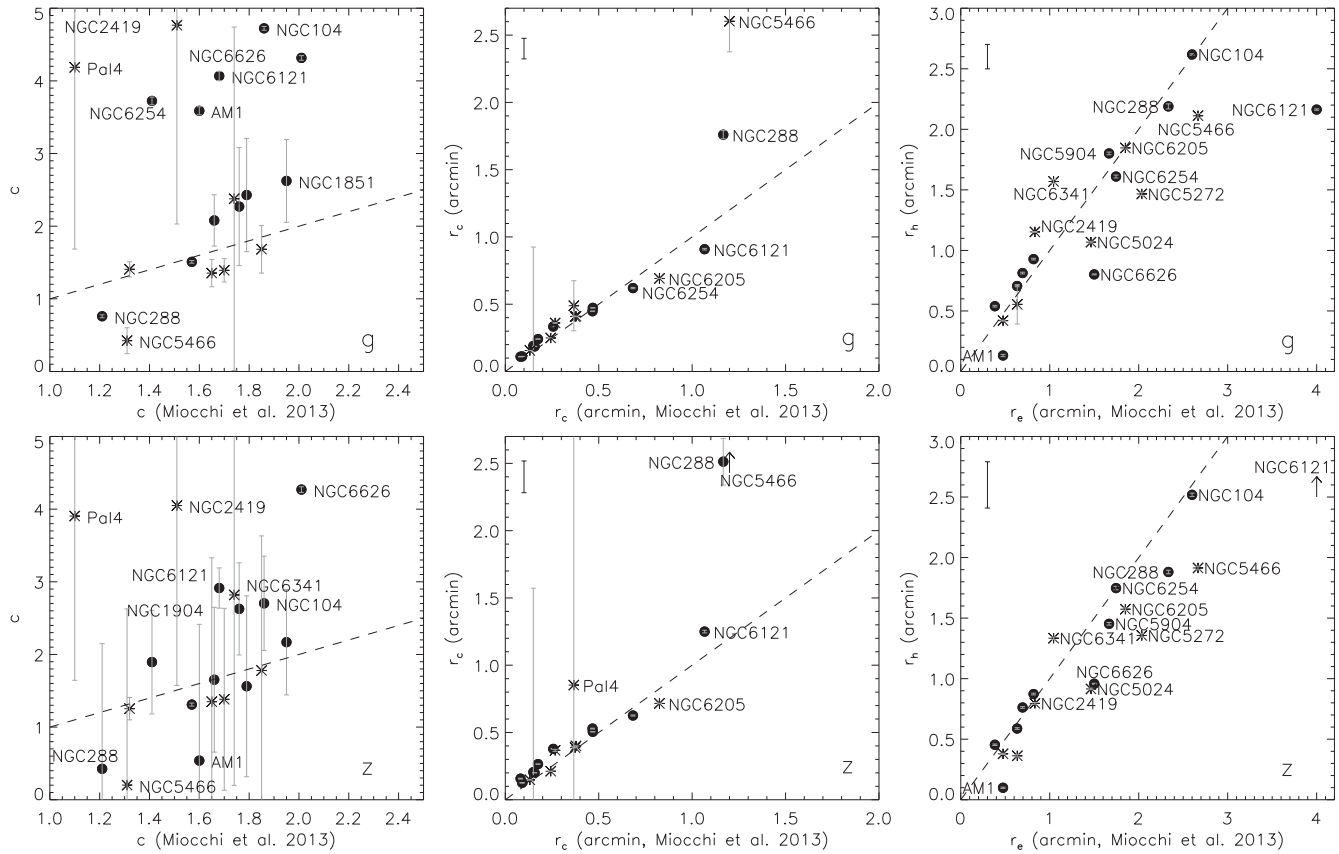

Figure 15. Comparison between our King model parameters (c, $r_{\rm c}$, $r_{\rm h}$) and the parameters based on King model fits to star count density profiles (Miocchi et al. 2013). The dashed line indicates the one-to-one correspondence. Concentrations higher than ∼2.5 are unreliable, which was also concluded based on the mock data in Fig. 5 and from Fig. 13.The black error bar in the top-left corner of each panel illustrates the systematic error given in Table 3.

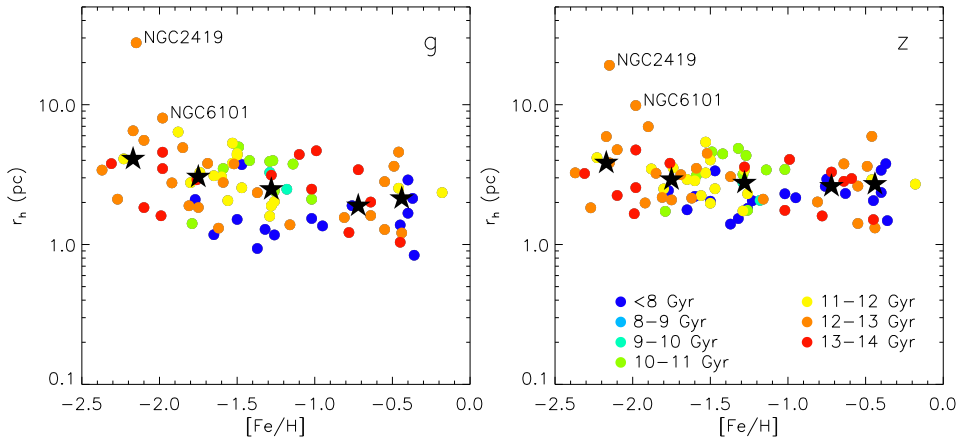

Figure 16. Correlation between r_h and [Fe/H]. The black filled stars present the median values for metallicity bins of 0.5 dex.

5 DISCUSSION

5.1 Correlations between size and metallicity

Several extragalactic studies found that red (metal-rich) GCs are systematically smaller (about 20 per cent) than blue (metal-poor) GCs (see e.g. Kundu & Whitmore 1998; Kundu et al. 1999; Puzia et al. 1999; Larsen et al. 2001). Larsen & Brodie (2003) argue that the difference is originated by a projection effect, due to a correlation between GC size and galactocentric distance, combined with different radial distributions of the metal-poor and metal-rich GC subpopulations (with the metal-rich GCs being more centrally located; see e.g. Kissler-Patig et al. 1997; Lee, Kim & Geisler 1998; Côté et al. 2001; Dirsch et al. 2003). At larger distances from the galactic centre, the projection effect is less strong, hence the trend should disappear in the galactic outskirts. However, Harris (2009) studied GCs from massive galaxies and found that the size differences between red and blue GCs remained at large distances. An alternative scenario was proposed by Jordán (2004), who advocate that the correlation between colour (metallicity) and r_h is a consequence of mass segregation and the longer lifetimes (for a given mass) of more metal-poor stars.

In Fig. 16, we show the half-light radii as a function of the metallicity (Harris 1996), colour-coded by age (which are largely obtained from Forbes & Bridges 2010, with some other references as described in Paper II). The correlation between both parameters is rather weak (Spearman's rank correlation coefficient is $\rho_{s,g} \sim -0.4$ with a significance level of 4.24×10^{-4} for the g band and $\rho_{s,z} \sim -0.23$ with a significance level of 3.12×10^{-2} for the z band). Nevertheless, Jordán (2004) stress that large samples are needed to accurately determine the *average* behaviour. Although Galactic GCs are not so numerous, we still try to recover the average behaviour by showing the median [Fe/H] and r_h in 0.5 dex metallicity bins. These median r_h values largely agree with the trend predicted by Jordán (2004): $r_{h,g}$ ∼4.1, 3.1, 2.5, 1.9 and 2.1 pc for the different metallicity bins ($r_{h,z}$ ∼3.8, 2.9, 2.8, 2.6 and 2.7 pc), thus the r_h difference between g and z band for the different metallicity bins is 0.3, 0.2, −0.3, −0.7 and −0.6 pc. However, the actual size differences are much larger than predicted by Jordán (2004). The interpretation of the trend between cluster size and iron abundance is not that straightforward. Therefore, we will revisit this issue in Section 5.3, where we discuss the correlation between the GC size and the Galactocentric distance.

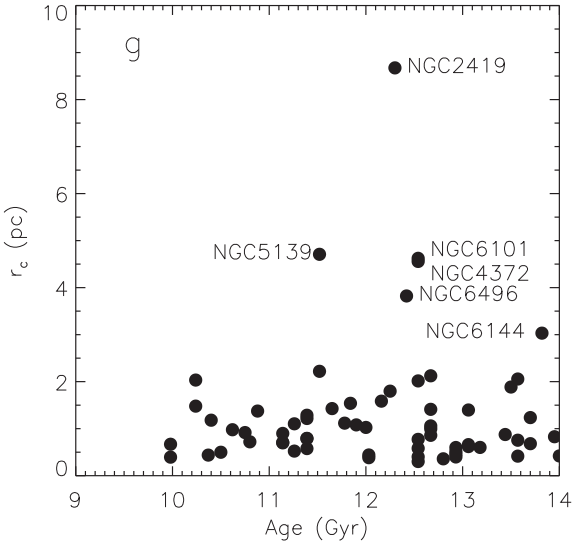

Figure 17. Correlation between age and r_c.

Note that for the g band, the youngest (i.e. <8 Gyr) clusters are systematically below the median values for the corresponding metallicity bin, while this is less clear for the z band.

5.2 Correlations between age and core radius

Mackey et al. (2008) found a trend between age and core radii for the GCs in the Small and Large Magellanic Clouds, with the young clusters (with ages between 10 Myr and 1 Gyr) showing a much smaller r_c spread than the old GCs (older than 1 Gyr). These authors investigated two physical processes leading to large-scale core expansion: mass-loss due to rapid stellar evolution in a primordially mass-segregated cluster and dynamical heating due to stellar mass black holes.

Galactic GCs are preferentially old (Forbes & Bridges 2010), hence one would expect to see a large range of r_c. However, Fig. 17 shows that the majority of the clusters have small g-band core radii. Mackey et al. (2008) believe this is a consequence of the positions of the GCs in the Galaxy: because a large fraction of the Milky Way GCs reside in the inner Galaxy, tidal forces are expected to rapidly destroy loosely bound clusters. The same conclusions can be drawn

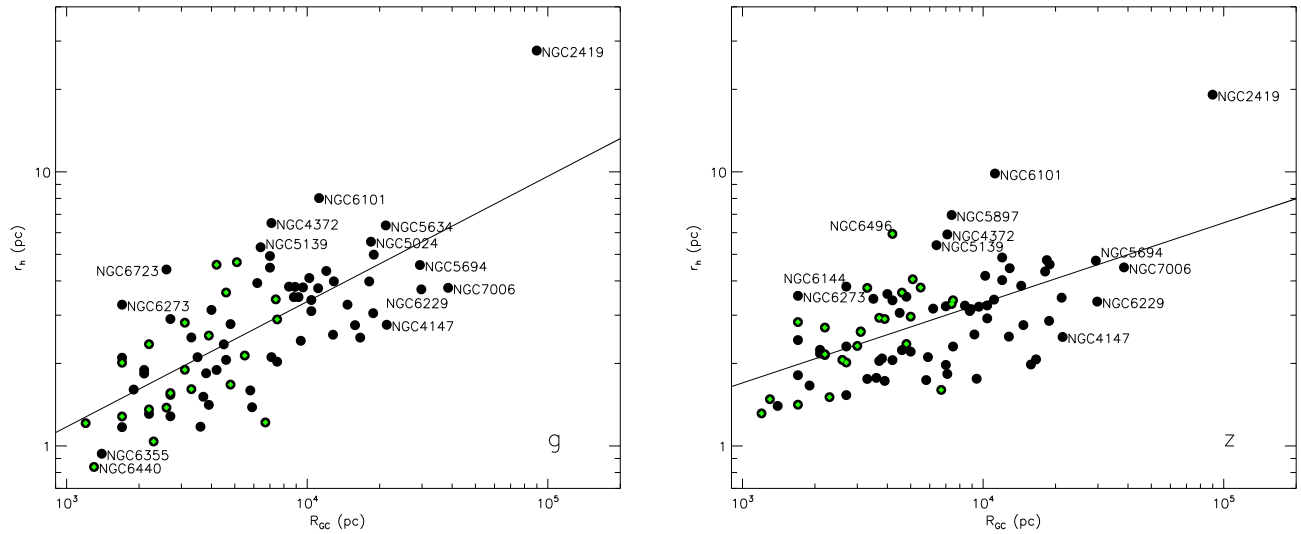

Figure 18. Correlation between the half-light radius r_h and the Galactocentric distance R_{GC} for the g and z band. Small green filled diamonds indicate the GCs with $[Fe/H] > -1$. The solid lines present robust fits to the data points of the clean sample (given by equations 2 and 3).

based on the z-band core radii. Both NGC 2419 and NGC 5139 (Omega Cen) have properties that hint to an extragalactic origin, which might explain their offset to the general trend.

5.3 Correlations with the Galactocentric distance

van den Bergh, Morbey & Pazder (1991) and McLaughlin (2000) have proposed the existence of a relation between the Galactocentric distance (R_{GC}) and the effective radius, arising from the tidal truncation [but see also Kundu et al. (1999)]. Recently Ernst & Just (2013) provide a more theoretical approach on the implications of the correlation between the half-mass and the galactocentric radius. Miocchi et al. (2013) recover this correlation and show that it does not depend on other cluster properties, confirming its likely dynamical origin. Puzia et al. (2014) studied the GC system of NGC 1399 and pointed at the influence of the GC orbit distribution on the evolution of the structural parameters. Fig. 18 shows the observed correlation between the half-light radius versus Galactocentric distance in our g- and z-band data. Based on a robust fit to the data points, we find:

$$\log r_h = -1.30 \pm 0.10 + (0.45 \pm 0.05) \times \log R_{GC} \quad (2)$$

for the g band (Spearmans rank correlation coefficient $\rho_{s,g}$ is about 0.68 with a significance level of 2.44×10^{-12}), which is in good agreement with the empirical power law found by van den Bergh et al. (1991) and Mackey & van den Bergh (2005), and in reasonable agreement with the scaling relation found by Miocchi et al. (2013). The latter study, though limited in sample size, covers several GCs at large R_{GC}.

Surprisingly, for the z band, we find:

$$\log r_h = -0.65 \pm 0.09 + (0.29 \pm 0.04) \times \log R_{GC}, \quad (3)$$

which is significantly different ($\rho_{s,z} \sim 0.53$, significance level $\sim 1.49 \times 10^{-7}$). To further investigate the origin of the offset, we made similar robust fits to the clean r- and i-band samples. We obtain:

$$\log r_h = -0.98 \pm 0.13 + (0.38 \pm 0.07) \times \log R_{GC} \quad (4)$$

for the r band ($\rho_{s,r} \sim 0.57$, significance level 7.71×10^{-5}) and

$$\log r_h = -0.76 \pm 0.12 + (0.33 \pm 0.06) \times \log R_{GC} \quad (5)$$

for the i band ($\rho_{s,i} \sim 0.60$, significance level 2.69×10^{-5}), hence we find evidence for a decreasing slope for redder bandpasses. Clusters are redder outwards, either because of tidal truncation or because shocks with the Galactic Centre environment speed up mass segregation. Colour gradients will be discussed in full detail in Section 5.5. It will become clear that the colour gradients are mainly caused by the influence of RGB stars and are not representative for the cluster count densities.

Georgiev & Böker (2014) find that nuclear star clusters (with sizes ranging between GC and UCD sizes) have smaller effective radii when measured in bluer filters. Now, we will study the size differences of GCs when measured in different filters, and we will try to link those differences to the discrepancy in the R_{GC}–r_h relations.

In Section 5.1, we found tentative evidence for the existence of a median size difference related to the cluster metallicity: metal-rich clusters, which are preferentially located close to the Galactic Centre, have larger r_h when measured in redder filters. Here, we define $\Delta r_{h,g-z}$ as the difference (in arcminutes) between the g- and z-band half-light radii. For the entire sample, the median (mean) of $\Delta r_{h,g-z}$ is about -0.06 arcmin (-0.07 arcmin, respectively), which is consistent with a zero difference within the errors. However, for GCs with R_{GC} lower than 5 kpc, the median (mean) of $\Delta r_{h,g-z}$ is about -0.19 arcmin (-0.23 arcmin, respectively), while for GCs at larger distances to the Galactic Centre, the median (mean) of $\Delta r_{h,g-z}$ is about 0.09 (0.08 arcmin, respectively). Therefore, close to the Galactic Centre, clusters have redder outskirts (or, equivalently, bluer centres). For GCs with $E(B-V) < 0.1$ ($E(B-V) \geq 0.1$), the median of $\Delta r_{h,g-z}$ is about 0.08 arcmin (-0.15 arcmin, respectively), hence GCs at low reddening appear larger in g than in z, while GCs at high reddening appear smaller in g than in z. Similar correlations are found when using the absolute distance above the Galactic plane instead of the extinction value.

To further scrutinize the effects of metallicity and tidal disruption on the cluster size, we make separate fits for the metal-rich and metal-poor subsamples of the clean sample. Because the metal-rich GCs do not span a wide range in Galactrocentric distances, we fix the slope of the relation to the value found in equations (2) and (3) and find that the intercept for metal-rich and metal-poor subsamples is not significantly different. This points to a scenario in which the origin of the size difference is related to the Galactocentric distance,

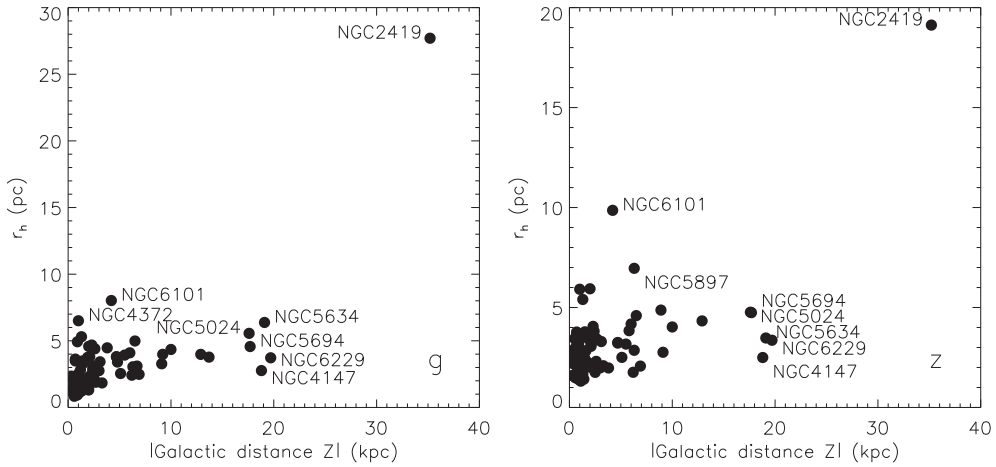

Figure 19. Correlation between the absolute distance above the Galactic plane and r_h.

and, not to [Fe/H] (hence in contrast to the tentative evidence found in Fig. 5.1).

Puzia et al. (2014) found a flattening of the $R_{GC} - r_h$ correlation in NGC 1399 beyond ∼20 kpc, while Miocchi et al. (2013) did not find evidence for a flattening of the latter relation in the outskirts of the Milky Way. Some GCs at ∼20 kpc with good fits are located below the general trend and could point at a flattening of the correlation. Nevertheless, the scatter on the correlation is significant.

To detect correlations between the deviation to the general trend and other parameters, we define

$$D_g = -1.30 + 0.45 \times \log(R_{GC}) - \log(r_h) \quad (6)$$

for the g band (and a similar definition for the z band; see van den Bergh 2012 for a similar approach). We searched for correlations between this new parameter and age, HB index, absolute magnitude and $[Fe/H]$, but did not find any significant trends and confirm therefore the purely dynamical origin of the correlation between r_h and R_{GC}, concurring with the recent literature (van den Bergh 2012; Miocchi et al. 2013). We also looked for correlations between the absolute distance D and the absolute distance to the Galactic plane, which could reveal some insights on the influence of tidal shocks during disc passages on the GC size. However, we did not find any clear trends.

Fig. 19 shows the correlation between the absolute distance above the Galactic plane and the half-light radii. The clusters located closer to the disc are generally smaller than those well above the Galactic plane, which can be ascribed to tidal stripping. For the g band, the Spearmans rank correlation coefficient $\rho_{s,g}$ is about 0.61 with a significance level of 2.66×10^{-9}. For the z band, the correlation is less strong; for the entire sample, we find $\rho_{s,z} \sim 0.46$ with a significance level of 8.66×10^{-6}.

5.4 Distributions of the structural parameters

The structural parameters of a cluster can be taken as a broad measure of its dynamical evolution. In Trager et al. (1995), the distribution of core radii of GCs was found to be bimodal, with about 20 per cent of clusters showing central light excesses consistent with core collapse. Cusps and similar excess light features appear to be relatively common in GCs in our Galaxy (Vesperini & Trenti 2010) and the Large Magellanic Cloud (Mackey & Gilmore 2003). In Fig. 20, we show the gz r_c distributions. We do not find clear signs for bimodality, in contrast to Trager et al. (1995).

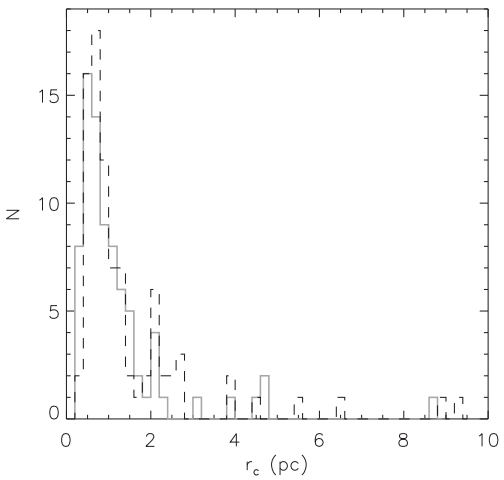

Figure 20. The g- (grey solid line) and z-band (black dashed line) distributions of the core radii.

Fig. 21 presents the gz distributions of the half-light radii. We find a median r_h of 2.7 pc (2.9 pc) for the g band (z band, respectively), which is in good agreement with $r_h \sim 3$ pc found for extragalactic GCs in the Virgo and Fornax clusters of galaxies (Jordán et al. 2005; Masters et al. 2010; see also e.g. fig. 16 of Puzia et al. 2014).

Standard dynamical models of GCs make clear predictions of the evolution of the ratio between the core and the half-light radii (see Trenti et al. 2010; Miocchi et al. 2013 and references therein). Fig. 22 presents the distribution of the ratio between the core and the half-light radii. We find a peaked distribution centred at $r_c/r_h \sim 0.4$, but do not recover the bimodal distribution found by Miocchi et al. (2013), with a peak in r_c/r_h at about 0.3. Both our and their r_c/r_h values are in agreement with expectations from simulations of cluster dynamical evolution.

5.5 Colour gradients

In galaxies, colour gradients are interpreted as a metallicity gradient (Tamura & Ohta 2000; La Barbera et al. 2010). If colour gradients exist in GCs, these would not be linked with the metallicity, as these objects have a largely homogenous metallicity (although variations in light element abundances are omnipresent). However, if dynamical processes affect stellar populations, for instance

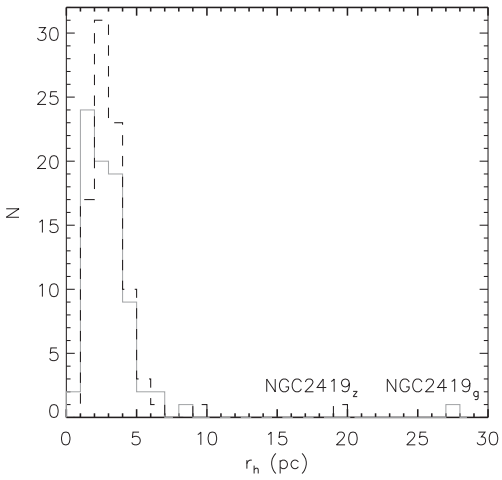

Figure 21. The *gz* distributions of the half-light radii. Legend as in Fig. 20.

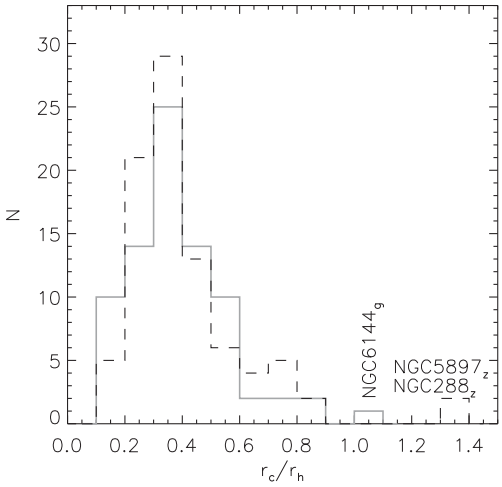

Figure 22. Distribution of the ratio between the core and the half-light radii. Legend as in Fig. 20.

through the creation of blue stragglers in cluster cores (Ferraro & Lanzoni 2009) or stripping of red giants to produce AGB-manque stars (Pasquato et al. 2013), the formation of cataclysmic variables, millisecond pulsars and intermediate mass black holes, we might be able to detect the presence of these objects through colour variations as a function of radius. Djorgovski & Piotto (1993) found that post-core-collapse clusters are bluer in their centre, and there were no colour gradients in the opposite direction. Djorgovski et al. (1991) found no blue cores in clusters with flat inner profiles, confirming the correlation between internal dynamics and stellar populations. This was attributed to the stripping of red giants in cluster cores to produce extended HBs (Pasquato et al. 2013) and the formation of blue stragglers by stellar collisions.

However, Sohn, Byun & Chun (1996) found colour gradients even in clusters that fitted the King profile and suggested that internal dynamics may produce extended HBs and lead to colour gradients. Sohn et al. (1998) also found both red and blue cores in both normal and post-core-collapse clusters. For example, unlike Djorgovski et al. (1991), Sohn et al. (1998) detect a red core in NGC 2808.

We find general flatness of the gradients beyond the half-light radius, which is somehow expected as we do not expect strong stellar population gradients. However, stronger gradients are apparent closer to the cluster centre. To study the colour of the cluster cores

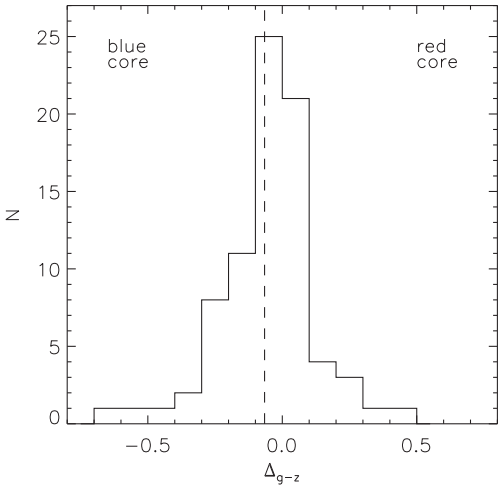

Figure 23. Distribution of Δ_{g-z} (defined in equation 7). The dashed line represents the median value of Δ_{g-z}. See text for more details.

and search for correlations with other GC parameters, we define a new parameter:

$$\Delta_{g-z} = (g-z)_{r_c} - (g-z)_{r_h}, \quad (7)$$

with $(g-z)_{r_c}$ the $g-z$ colour at the average *gz* core radius (similar for the half-light radius). This parameter is negative for blue cores and positive for red cores.

In Fig. 23, we present the distribution of this newly defined parameter, which is rather symmetric. Clusters with extremely positive values ($\Delta_{g-z} > 0.3$) are NGC4833 and NGC6584, extremely negative values ($\Delta_{g-z} < -0.4$) are found for NGC6235, NGC6352 and NGC6681. These clusters are close to the Galactic disc or bulge, which results in SB profiles polluted by Milky Way stars and complicates the determination of the structural parameters.

Clusters in the 'blue core tail' (with $-0.4 \leq \Delta_{g-z} \leq -0.2$) are NGC 6121, NGC 6342, NGC 6453, NGC 6535, NGC 6638, NGC 6637, NGC 6642, NGC 6712, NGC 6864 and NGC 6981. Clusters in the 'red core tail' (with $0.1 \leq \Delta_{g-z} \leq 0.3$) are NGC 2298, NGC 5634, NGC 6171, NGC 6273, NGC 6341, NGC 6760 and NGC 6779. For a fraction of these clusters, we also determined the King parameters based on a SB profile centred with the RGB method, a procedure which should not be susceptible towards centrally located bright stars (see Section 3.3). About one-third of the 'tail' clusters are located towards the Galactic bulge, prohibiting an RGB-based centre determination. For a couple of clusters, only poor colour–magnitude diagrams were obtained and a centre determination based on the RGB was not possible.

It is generally difficult to study colour gradients, especially close to the cluster centre, because only a couple of stochastically distributed RGB stars can alter the SB profiles and originate colour gradients. This is especially true for low-density clusters, but can also affect clusters as bright as NGC 104: RGB stars and poor centring can affect the resulting King parameters drastically.

6 SUMMARY

As a part of the G2C2 project, we use in the current study our optical data set (presented in Paper I) to derive structural parameters fitting King (1962) models to the GC SB profiles. We present structural parameters in the *g* and *z* filters for 111 Galactic GCs, while we also include *r*- and *i*-band values for 60 clusters and *u*-band estimates for 22 GCs. For some clusters, it was not possible to fit a representative

King model to the SB profiles. Neglecting the unrealistic fits (judged by visual inspection), we present u, g, r, i and z structural parameters for 18, 94, 50, 48 and 95 GCs, respectively. Nevertheless, in order to maintain the focus on the GCs with soundly determined parameters in the discussion, we find it necessary to introduce some parameter criteria in the discussion (Section 4). For the u (g, r, $i$and$z$) band, the structural parameters of 12, (80, 41, 42 and 87, respectively) GCs satisfy these standards.

Because the bulk of our data set was obtained with CTIO 0.9 m telescope observations, suffering from a limited FOV, we extensively discuss the effects of a limited field-of-view on the derived King model parameters. In general, the resulting core radii are in good comparison with the current literature values. However, our half-light radii are slightly underestimated when compared to the literature. The concentrations (and therefore also the tidal radii) are poorly constrained, partly due to the limited radial extent of our SB profiles. Moreover, RGB stars are biasing the centring procedure and can provoke strong central SB cusps, which further contribute to the overestimation of the concentration parameter. The issues related to these bright stars are scrutinized based on our photometric data and simulated clusters. Logically, the effects of the randomly distributed RGB stars on the fitted King models are stronger in sparsely populated clusters, for which a star count density approach is recommended. Colour gradients are examined and can also be related to RGB stars.

We recover the known relation between the half-light radius and the Galactocentric distance for the g band, but find a lower slope for redder filters. We did not find a correlation between the scatter on this relation and other cluster properties. We find tentative evidence for a correlation between the half-light radii and [Fe/H], with metal-poor GCs being larger than metal-rich GCs. However, it turns out that this trend is due to the relation between the half-light radius and the Galactocentric distance, with metal-rich clusters being more centrally located than metal-poor clusters.

ACKNOWLEDGEMENTS

The authors acknowledge the anonymous referee for very useful comments and suggestions. JV acknowledges the support of ESO through a studentship. JV and MB acknowledge the support of the Fund for Scientific Research Flanders (FWO-Vlaanderen). The authors are grateful to CTIO for the hospitality and the dedicated assistance during the numerous observing runs.

REFERENCES

Ahn C. P. et al., 2012, ApJS, 203, 21
Alexander P. E. R., Gieles M., 2013, MNRAS, 432, L1
Alonso-García J., Mateo M., Sen B., Banerjee M., von Braun K., 2011, AJ, 141, 146
Bahcall J. N., Soneira R. M., 1980, ApJS, 44, 73
Bellazzini M., 2007, A&A, 473, 171 (B07)
Benacquista M. J., Downing J. M. B., 2013, Living Rev. Relativ., 16, 4
Bevington P. R., Robinson D. K., 1992, Data Reduction and Error Analysis for the Physical Sciences. McGraw-Hill, New York
Bianchini P., Varri A. L., Bertin G., Zocchi A., 2013, ApJ, 772, 67
Brodie J. P., Strader J., 2006, ARA&A, 44, 193
Cohn H., 1980, ApJ, 242, 765
Correnti M., Bellazzini M., Dalessandro E., Mucciarelli A., Monaco L., Catelan M., 2011, MNRAS, 417, 2411
Côté P. et al., 2001, ApJ, 559, 828
de Souza R. E., Gadotti D. A., dos Anjos S., 2004, ApJS, 153, 411
Dirsch B., Richtler T., Geisler D., Forte J. C., Bassino L. P., Gieren W. P., 2003, AJ, 125, 1908
Djorgovski S., King I. R., 1986, ApJ, 305, L61
Djorgovski S., Piotto G., 1993, in Djorgovski S. G., Meylan G., eds, ASP Conf. Ser. Vol. 50, Structure and Dynamics of Globular Clusters. Astron. Soc. Pac., San Francisco, p. 203
Djorgovski S., Piotto G., Phinney E. S., Chernoff D. F., 1991, ApJ, 372, L41
Elson R. A. W., Fall S. M., Freeman K. C., 1987, ApJ, 323, 54
Ernst A., Just A., 2013, MNRAS, 429, 2953
Fabricius M. H. et al., 2014, ApJ, 787, L26
Ferraro F. R., Lanzoni B., 2009, Rev. Mex. Astron. Astrofis, 37, 62
Ferraro F. R., Paltrinieri B., Rood R. T., Dorman B., 1999, ApJ, 522, 983
Ferraro F. R., Possenti A., Sabbi E., Lagani P., Rood R. T., D'Amico N., Origlia L., 2003, ApJ, 595, 179
Forbes D. A., Bridges T., 2010, MNRAS, 404, 1203
Frank M. J., Hilker M., Baumgardt H., Ct P., Grebel E. K., Haghi H., Kpper A. H. W., Djorgovski S. G., 2012, MNRAS, 423, 2917
Fregeau J. M., Rasio F. A., 2007, ApJ, 658, 1047
Fregeau J. M., Joshi K. J., Portegies Zwart S. F., Rasio F. A., 2002, ApJ, 570, 171
Fusi Pecci F., Ferraro F. R., Corsi C. E., Cacciari C., Buonanno R., 1992, AJ, 104, 1831
Gadotti D. A., 2008, MNRAS, 384, 420
Georgiev I. Y., Böker T., 2014, MNRAS, 441, 3570
Gieles M., Baumgardt H., Heggie D. C., Lamers H. J. G. L. M., 2010, MNRAS, 408, L16
Goldsbury R., Heyl J., Richer H., 2013, ApJ, 778, 57
Grillmair C. J., Freeman K. C., Irwin M., Quinn P. J., 1995, AJ, 109, 2553
Harris W. E., 1996, AJ, 112, 1487
Harris W. E., 2009, ApJ, 699, 254
Heggie D., Hut P., 2003, The Gravitational Million-Body Problem: A Multidisciplinary Approach to Star Cluster Dynamics. Cambridge Univ. Press, Cambridge
Hernandez X., Jiménez M. A., Allen C., 2013, MNRAS, 428, 3196
Hurley J. R., Shara M. M., 2012, MNRAS, 425, 2872
Jordán A., 2004, ApJ, 613, L117
Jordán A. et al., 2005, ApJ, 634, 1002
Jordán A. et al., 2009, ApJS, 180, 54
Jordi K., Grebel E. K., 2010, A&A, 522, A71
Kacharov N. et al., 2014, A&A, 567, A69
King I., 1962, AJ, 67, 471
King I. R., 1966, AJ, 71, 64
Kissler-Patig M., Kohle S., Hilker M., Richtler T., Infante L., Quintana H., 1997, A&A, 319, 470
Kundu A., Whitmore B. C., 1998, AJ, 116, 2841
Kundu A., Whitmore B. C., Sparks W. B., Macchetto F. D., Zepf S. E., Ashman K. M., 1999, ApJ, 513, 733
La Barbera F., De Carvalho R. R., De La Rosa I. G., Gal R. R., Swindle R., Lopes P. A. A., 2010, AJ, 140, 1528
Larsen S. S., Brodie J. P., 2003, ApJ, 593, 340
Larsen S. S., Brodie J. P., Huchra J. P., Forbes D. A., Grillmair C. J., 2001, AJ, 121, 2974
Lee M. G., Kim E., Geisler D., 1998, AJ, 115, 947
Lin D., Irwin J. A., Webb N. A., Barret D., Remillard R. A., 2013, ApJ, 779, 149
Lützgendorf N. et al., 2013, A&A, 552, A49
Mackey A. D., Gilmore G. F., 2003, MNRAS, 338, 85
Mackey A. D., van den Bergh S., 2005, MNRAS, 360, 631
Mackey A. D., Wilkinson M. I., Davies M. B., Gilmore G. F., 2008, MNRAS, 386, 65
McLaughlin D. E., 2000, ApJ, 539, 618
McLaughlin D. E., van der Marel R. P., 2005, ApJS, 161, 304
Masters K. L. et al., 2010, ApJ, 715, 1419
Miocchi P. et al., 2013, ApJ, 774, 151
Newell B., Oneil E. J., Jr, 1978, ApJS, 37, 27
Noyola E., Gebhardt K., 2006, AJ, 132, 447
Odenkirchen M. et al., 2001, ApJ, 548, L165

Olszewski E. W., Saha A., Knezek P., Subramaniam A., de Boer T., Seitzer P., 2009, AJ, 138, 1570
Pasquato M., Raimondo G., Brocato E., Chung C., Moraghan A., Lee Y.-W., 2013, A&A, 554, A129
Peng C. Y., Ho L. C., Impey C. D., Rix H.-W., 2002, AJ, 124, 266
Peng C. Y., Ho L. C., Impey C. D., Rix H.-W., 2010, AJ, 139, 2097
Press W. H., Schechter P., 1974, ApJ, 187, 425
Puzia T. H., Kissler-Patig M., Brodie J. P., Huchra J. P., 1999, AJ, 118, 2734
Puzia T. H., Paolillo M., Goudfrooij P., Maccarone T. J., Fabbiano G., Angelini L., 2014, ApJ, 786, 78
Salinas R., Jílková L., Carraro G., Catelan M., Amigo P., 2012, MNRAS, 421, 960
Schlafly E. F., Finkbeiner D. P., 2011, ApJ, 737, 103
Simunovic M., Puzia T. H., 2014, ApJ, 782, 49
Smith J. A. et al., 2002, AJ, 123, 2121
Sohn Y.-J., Byun Y.-I., Chun M.-S., 1996, Ap&SS, 243, 379
Sohn Y.-J., Byun Y.-I., Yim H.-S., Rhee M.-H., Chun M.-S., 1998, J. Astron. Space Sci., 15, 1
Sollima A., Martínez-Delgado D., Valls-Gabaud D., Peñarrubia J., 2011, ApJ, 726, 47
Stetson P. B., 1987, PASP, 99, 191
Tamura N., Ohta K., 2000, AJ, 120, 533
Trager S. C., King I. R., Djorgovski S., 1995, AJ, 109, 218
Trenti M., Vesperini E., Pasquato M., 2010, ApJ, 708, 1598
van den Bergh S., 2012, ApJ, 746, 189
van den Bergh S., Morbey C., Pazder J., 1991, ApJ, 375, 594
VandenBerg D. A., Brogaard K., Leaman R., Casagrande L., 2013, ApJ, 775, 134
Vanderbeke J. et al., 2014a, MNRAS, 437, 1725 (Paper I)
Vanderbeke J. et al., 2014b, MNRAS, 437, 1734 (Paper II)
Vesperini E., Chernoff D. F., 1994, ApJ, 431, 231
Vesperini E., Trenti M., 2010, ApJ, 720, L179
Wang S., Ma J., 2013, AJ, 146, 20
Wilson C. P., 1975, AJ, 80, 175
York D. G. et al., 2000, AJ, 120, 1579

SUPPORTING INFORMATION

Additional Supporting Information may be found in the online version of this article:

Vanderbeke2015_G2C2III_King_structural_parameters_online_tables.pdf
Vanderbeke2015_G2C2III_King_SB_profiles_SDSS.pdf
Vanderbeke2015_G2C2III_King_SB_profiles_CTIO.pdf
(http://mnras.oxfordjournals.org/lookup/suppl/doi:10.1093/mnras/stv850/-/DC1).

Please note: Oxford University Press are not responsible for the content or functionality of any supporting materials supplied by the authors. Any queries (other than missing material) should be directed to the corresponding author for the paper.

This paper has been typeset from a TEX/LATEX file prepared by the author.